Molecular Cell
Article

# Polypyrimidine Tract Binding Protein Stabilizes the Encephalomyocarditis Virus IRES Structure via Binding Multiple Sites in a Unique Orientation

Panagiota Kafasla,[1] Nina Morgner,[2] Tuija A.A. Pöyry,[1] Stephen Curry,[3] Carol V. Robinson,[2] and Richard J. Jackson[1,*]
[1]Department of Biochemistry, University of Cambridge, Cambridge CB2 1GA, UK
[2]Department of Chemistry, University of Cambridge, Cambridge CB2 1EW, UK
[3]Division of Cell and Molecular Biology, Department of Life Sciences, Imperial College, London SW7 2AZ, UK
*Correspondence: rjj@mole.bio.cam.ac.uk
DOI 10.1016/j.molcel.2009.04.015

## SUMMARY

**Polypyrimidine tract binding (PTB) protein is a regulator of alternative pre-mRNA splicing, and also stimulates the initiation of translation dependent on many viral internal ribosome entry segments/sites (IRESs). It has four RNA-binding domains (RBDs), but although the contacts with many IRESs have been mapped, the orientation of binding (i.e., which RBD binds to which site in the IRES) is unknown. To answer this question, 16 derivatives of PTB1, each with a single cysteine flanking the RNA-binding surface in an RBD, were constructed and used in directed hydroxyl radical probing with the encephalomyocarditis virus IRES. The results, together with mass spectrometry data on the stoichiometry of PTB binding to different IRES derivatives, show that the minimal IRES binds a single PTB in a unique orientation, with RBD1 and RBD2 binding near the 3′ end, and RBD3 contacting the 5′ end, thereby constraining and stabilizing the three-dimensional structural fold of the IRES.**

## INTRODUCTION

Soon after its discovery as a nuclear protein with high affinity for intronic pyrimidine-rich tracts in pre-mRNA, polypyrimidine tract binding (PTB) protein, also known as hnRNPI, was recognized to be an important regulator of alternative splicing (reviewed in Valcarcel and Gebauer, 1997; Sawicka et al., 2008). It was noted that although hnRNPI is predominantly located in the nucleus, there is considerably more in the cytoplasm than is typical of hnRNPs, implying that it is probably a shuttling protein (Ghetti et al., 1992). Indeed, an influence of PTB on several different cytoplasmic events has been reported, for example the localization of certain mRNAs and the stability of others (reviewed in Sawicka et al., 2008). However, the best known cytoplasmic function is the stimulation of translation initiation dependent on picornaviral internal ribosome entry sites/segments (IRESs), which was discovered very soon after PTB was first characterized (reviewed in Jackson and Kaminski, 1995). Subsequently, PTB has been reported to stimulate the activity of many cellular mRNA IRESs, and it has even been suggested that PTB may be a general *trans*-acting factor for IRES-dependent initiation (Sawicka et al., 2008).

The PTB requirement for picornavirus IRESs varies quite widely according to the species. It is absolutely required for all of the Type I (entero- and rhinovirus) IRESs that have been tested (Hunt and Jackson, 1999), but Type II picornavirus IRESs show more variability: the foot-and-mouth disease virus (FMDV) IRES shows strong dependency on PTB (Niepmann, 1996; Pilipenko et al., 2000), but for the encephalomyocarditis virus (EMCV) IRES, the PTB requirement is conditional on the nature of the reporter and the IRES variant used (Kaminski and Jackson, 1998), whereas there are conflicting reports for Theiler's murine encephalomyelitis virus (TMEV), ranging from no dependency to quite strong stimulation (Kaminski et al., 1995; Pilipenko et al., 2001), which is likely to be due to the use of different strains.

PTB has four RNA-binding domains (RBDs) of the RNP1/RNP2 class, although the amino acid sequences of these motifs in PTB are somewhat noncanonical. Alternative splicing results in two variants of the prototypic PTB1: PTB2 and PTB4, which differ from PTB1 by the insertion of 19 or 26 amino acids, respectively, in the linker between RBD2 and RBD3. The hierarchy of efficiency of these in an alternative splicing assay (PTB4 > PTB2 > PTB1) was almost precisely the opposite from their hierarchy in promoting initiation on the human rhinovirus IRES (Wollerton et al., 2001). PTB1 was initially considered to form dimers in solution via interactions involving the RBD2 region, but it is now known to be a monomer with a somewhat extended conformation (Monie et al., 2005).

Although the interaction of PTB with viral IRESs has been extensively studied by gel-shift and UV-crosslinking assays, and its binding sites on Type II IRESs have been mapped by footprinting (Kolupaeva et al., 1996; Pilipenko et al., 2000, 2001), nothing is known about the details of how it is docked onto these IRESs: the question of which RBD binds to which part of the IRES. Because it has proved impossible (so far) to address this question by X-ray crystallography or NMR spectroscopy of PTB/IRES complexes, we turned to directed hydroxyl radical probing. In this approach, an Fe(II)-EDTA moiety is attached to a strategically placed site in a given RBD, and after forming the PTB/RNA complex, hydroxyl radicals are generated at the Fe(II) by the Fenton reaction. These radicals cause RNA backbone cleavage, irrespective of structure or sequence, but

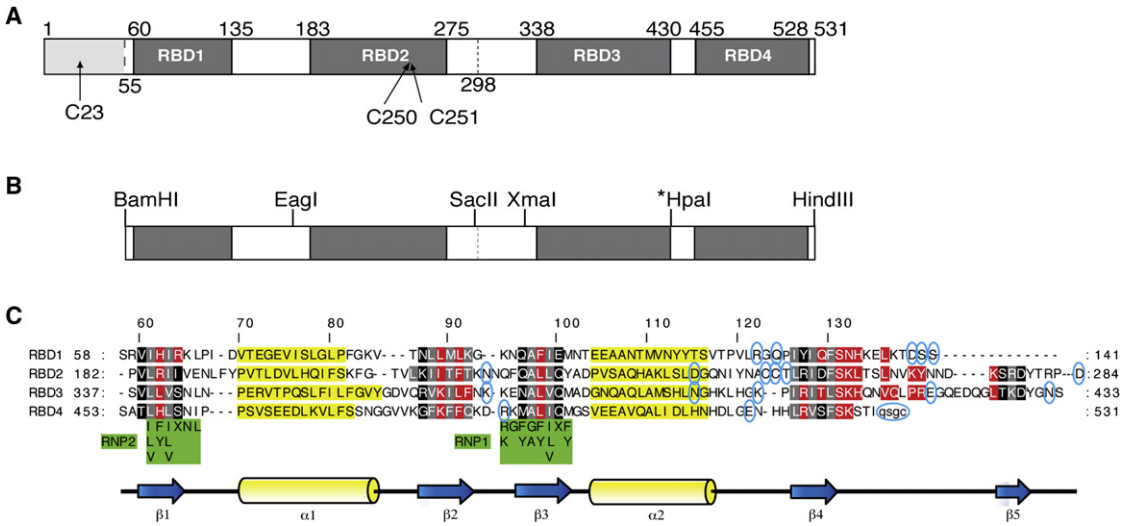


**Figure 1. Generation of Cys Replacement Mutants of PTB**

(A) Schematic representation of PTB1 showing the positions of the four RBDs and the Cys residues. Residues 1–54, which are deleted in ΔNTD-PTB, identical to PTB1-1234 of Monie et al. (2005), are shown by light shading. The position (residue 298) at which PTB2 and PTB4 have inserts of 19 or 26 additional amino acids is also shown.

(B) Schematic diagram of the ΔNTD-PTB starting construct, with Cys-250 and -251 both mutated to serine. The unique restriction sites used to exchange individual RBDs between mutants are shown; the asterisked HpaI site was introduced by a silent mutation.

(C) Sequence alignment of the four RBDs of PTB, adapted from Oberstrass et al. (2005) with the same color coding: amino acid residues interacting with the RNA are shown in red; residues in black and gray are located in the β sheets, with those in gray pointing toward the hydrophobic core of the RBD; and residues highlighted in yellow are in the α helices. The consensus RNP1 and RNP2 sequences are shown below in green. The residues mutated to Cys for subsequent conjugation with Fe(II)-BABE are circled. The four C-terminal residues in lower case represent the extension of the protein that was made in order to create a Cys residue sufficiently downstream of RBD4.

because they are very short lived, cleavage is limited to sites in close proximity to the Fe(II), facilitating identification of which RNA segment is nearest that particular RBD (Culver and Noller, 2000). The EMCV IRES was chosen for these studies, because it is the best characterized IRES in terms of its secondary structure and known PTB-binding sites; thus, it provides a good platform for validating the experimental approach.

## RESULTS

### Design, Assay, and Derivatization of PTB Mutants

PTB1 (hereafter designated simply PTB) has three Cys residues: Cys-23 in the N-terminal domain, and the other two (Cys-250, Cys-251) in RBD2 (Figure 1A). All of the mutants described here were generated in the background of the construct PTB1-1234 described by Monie et al. (2005), renamed ΔNTD-PTB for this work: this has an N-terminal His tag and is lacking the N-terminal (amino acids 1–54) domain (Figure 1B), which has the nuclear import/export signals but plays no role in RNA binding. First, C250S and C251S mutations were made, separately and together, the latter generating a construct encoding a Cys-less protein, which was an important control used routinely in all of the probing assays. Single Cys residues were then introduced into the Cys-less background at various positions (Figure 1C), which were chosen on the basis of the published NMR structures of each RBD complexed with an oligonucleotide ligand (Oberstrass et al., 2005). The aim was to place the cysteines far enough away from the actual RNA-binding surface that the conjugated Fe-BABE moiety would be unlikely to cause steric interference with RNA binding, but in positions flanking the RNA-binding surface such that the Fe of the Fe(II)-BABE would probably be in close proximity to the bound RNA. Because the RNA-binding surface of RBD4 extends almost to the very C terminus of the protein, we chose to introduce a Cys downstream of this RBD by extending the protein with GSGC, rather than by point mutation.

Each mutant was then tested for its ability to promote translation initiation on the EMCV IRES in a variant of the PTB-depleted reticulocyte lysate system described previously (Kaminski et al., 1995). For these functional assays, we used a mutant EMCV IRES with an expanded 7A bulge at the three-way junction in the J-K domain (see Figure 3C), because this shows a greater response to PTB than the wild-type IRES with a 6A bulge (Kaminski and Jackson, 1998), but a wild-type (6A) IRES was used for the probing assays, except where otherwise stated. Figure 2A shows that removing the N-terminal domain and mutating C250 and C251 to serines had no effect on the stimulation of translation by PTB, and representative assays of some Cys substitution mutants are shown in Figure 2B. A minimum of two, and in some cases up to four, different mutant PTB concentrations (maximum 180 nM) were used with a constant mRNA concentration of 20 nM. In most cases, stimulation of translation was evident even at the lowest PTB concentration (22.5 nM), and it reached a maximum at 90 nM added PTB (a PTB/IRES molar ratio of 4.5). The stimulation at each concentration of mutant ΔNTD-PTB was determined relative to wild-type (FL) PTB. The

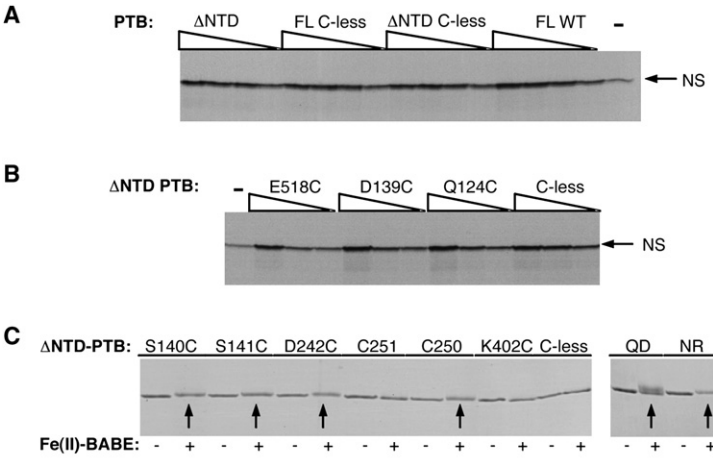


D

| | | translation efficiency - BABE | translation efficiency + BABE | derivatization efficiency |
|---|---|---|---|---|
| **Starting constructs** | **FL-WT-PTB (C23/C250/C251)** | 100 | 90 | n/a |
| | **FL-PTB-C23S (C250/C251)** | 80 | 77 | n/a |
| | **FL-PTB-C250S/C251S (C23)** | 75 | 88 | n/a |
| | **FL C-less (** C23S/C250S/C251S) | 78 | 72 | - |
| | **ΔNTD-PTB (WT)** | 93 | 87 | n/a |
| | **ΔNTD-C-less PTB** (C250S/C251S) | 87 | 81 | - |
| **RBD1 mutants** in ΔNTD-PTB | **PTB-R122C** | 92 | 81 | - |
| | **PTB-Q124C** | 97 | 68 | + |
| | **PTB-D139C** | 76 | 61 | ++ |
| | **PTB-S140C** | 100 | 89 | ++ |
| | **PTB-S141C** | 94 | 81 | ++ |
| **RBD2 mutants** in ΔNTD-PTB | **PTB-N219C** | 71 | 82 | ++ |
| | **PTB-D242C** | 97 | 79 | ++ |
| | **PTB-C250** | 95 | 94 | ++ |
| | **PTB-C251** | 102 | 87 | - |
| | **PTB-T252C** | 94 | 84 | + |
| | **PTB-D284C** | 114 | 125 | ++ |
| **RBD3 mutants** in ΔNTD-PTB | **PTB-K373C** | 118 | 114 | ++ |
| | **PTB-N395C** | 71 | 65 | ++ |
| | **PTB-K402C** | 108 | 95 | - |
| | **PTB-E419C** | 84 | 68 | ++ |
| | **PTB-N432C** | 81 | 59 | ++ |
| **RBD4 mutants** in ΔNTD-PTB | **PTB-R491C** | 87 | 84 | ++ |
| | **PTB-E518C** | 96 | 87 | ++ |
| | **PTB-I531GSGC** | 87 | 76 | + |
| **Multiple mutations** | **PTB-QD** (Q124C/D284C) | 94 | 86 | * |
| | **PTB-NR** (N395C/R491C) | 100 | 91 | * |
| | **PTB-QDNR** | 90 | 80 | * |

**n/a** not used in the present study
***** as expected from results for individual mutations
**++** ~100% derivatization
**+** partial derivatization
**-** no detectable derivatization

**Figure 2. Representative Assays of PTB Derivatives for Stimulation of EMCV IRES Activity and Reaction with Fe(II)-BABE**

(A) Assay of wild-type full-length PTB (FL WT), the ΔNTD-PTB truncation mutant, and their Cys-less derivatives (FL C-less, ΔNTD C-less). Uncapped monocistronic mRNA (20 nM) with the EMCV IRES linked to influenza virus NS coding sequences was translated in PTB-depleted lysate (–), and in depleted lysate supplemented with purified recombinant hexahistidine-tagged PTB proteins at a final concentration of 22.5, 45, 90, and 180 nM. Translation products were analyzed by SDS-PAGE, and the resulting autoradiograph is shown.

(B) Assay of the designated mutant derivatives of ΔNTD-PTB under the same conditions, except that the recombinant His-tagged proteins were at a final concentration of 22.5, 45, and 90 nM.

(C) Reaction of selected His-tagged ΔNTD-PTB mutants with Fe(II)-BABE. After reaction and removal of excess Fe(II)-BABE, 400 ng each derivatized protein (+) was analyzed by SDS-PAGE alongside the same amount of the corresponding nonderivatized protein (–). The Coomassie (brilliant blue R250)-stained gel is shown, with arrows highlighting those mutants showing a significant mobility shift after derivatization.

(D) Summary of translation assay and derivatization assay results for all mutants.

averages of these relative efficiency values for each mutant are presented in Figure 2D; all retained significant activity (>70% of full-length PTB) in promoting IRES-dependent translation.

Next, the single Cys mutants were conjugated with Fe(II)-BABE under standard conditions (Culver and Noller, 2000; Marzi et al., 2003). Initially, we assessed derivatization efficiency by using the fluorescent –SH reagent (see Supplemental Data, available online) described by Culver and Noller (2000), but we noted that conjugation with Fe(II)-BABE resulted in a sufficient change of mobility on SDS-PAGE (shown for a representative set of mutants in Figure 2C) to provide a better way of assessing the extent of the reaction. Three of the 19 single Cys derivatives (R122C, C251, K402C) did not react at all with Fe-BABE; mutants Q124C, T252C, and I531GSGC were found to react partially (~60%), but the other 13 all showed close to 100% derivatization (Figure 2D). All of the derivatized proteins retained significant activity (>60% relative to full-length, wild-type, unmodified PTB) in stimulating translation dependent on the EMCV IRES (Figure 2D).

We also combined some of the mutants in pairs, with each Cys in a different RBD: (a) Q124C in RBD1 and D284C in RBD2 ("QD"); and (b) N395C in RBD3 and R491C in RBD4 ("NR"). These two were also combined to generate "QDNR" with four Cys, one in each RBD. All three of these multiple PTB mutants were functional in the in vitro translation assay (Figure 2D). The derivatization efficiency was exactly as expected from results with the two (or four) individual single Cys mutations (Figures 2C and 2D), as were the RNA cleavage sites, although fragment band intensity was slightly reduced (Figures 3A and 3B).

## Directed Hydroxyl Radical Probing of the EMCV IRES

The Fe(II)-BABE PTB derivatives, as well as the mock-conjugated Cys-less control, were preincubated at 37°C with the 5′ or 3′ end $^{32}$P-labeled IRES probe for 20 min, then ascorbic acid and hydrogen peroxide were added, and incubation continued for 30 min on ice, before the reaction was quenched by phenol extraction of the RNA fragments. Representative examples of the RNA product analysis gels with each type of end-labeled probe are shown in Figures 3A and 3B, respectively.

Although the input RNA was overwhelmingly intact (full-length probe), a number of fragments appeared after addition of hydrogen peroxide and ascorbic acid, either in the absence of any protein or in the presence of the Cys-less PTB (Figure 3). The bands in the Cys-less lane were treated as the background, and bands in lanes with Fe(II)-PTB mutants were taken to be genuine products of hydroxyl radical cleavage only if they were entirely absent from the Cys-less control lane (or were present, but at decidedly lower intensity).

For the first experiments, the probe encompassed nt 260–849 of the EMCV virion RNA sequence in the numbering of Duke et al. (1992), representing the complete 5′UTR downstream of the polyC tract, plus the first 16 nt of the viral coding sequence. As shown in Figure 3C, this segment is conventionally regarded as consisting of nine secondary structure domains (Domains D–L, inclusive), of which Domains D–G make only a minor contribution to IRES function, whereas Domains H–L are essential (Jang and Wimmer, 1990; Duke et al., 1992). With our standard RNA probe concentration of 50 nM, appreciable backbone cleavage was generally seen at equimolar Fe(II)-PTB/IRES, and a maximum signal was seen with a molar ratio of 2, although there were some exceptions that will be discussed later. For the majority of sites, raising the Fe(II)-PTB/RNA ratio much above 2-fold did not result in any increase in the intensity of the genuine cleavage product bands; rather, the background smear increased in intensity, and the relative proportion of full-length uncleaved probe decreased, especially at 8- to 10-fold molar excess (see, for example, Figures 5A–5C; Figure S2B). As this loss of full-length probe at high PTB/RNA input was much less evident with the Cys-less mutant (Figure 5A; Figure S2B), we consider it most likely to be due to nonspecific cleavages (i.e., dependent on the conjugated Fe-BABE and the consequent Fenton reaction) resulting from random interaction of the excess PTB with the RNA, rather than nuclease contamination of the PTB preparations.

To estimate the relative efficiency of cleavage at any particular site, the first step was to eliminate any loading variation between lanes, by determining the intensities of a given band in the Fe(II)-PTB lane and of the equivalent region of the Cys-less control lane, and normalizing these values with respect to the corresponding full-length uncleaved probe band or (more usually) to other background bands whose intensity was found to vary between lanes in parallel with the full-length probe yield (Figures 3A and 3B). After subtracting the relevant normalized Cys-less background value, the calculated net cleavage efficiency indices for all cleavage product bands were ranked, and the ranking list was divided into three groups (representing strong, medium, and weak cleavages) following common practice (Culver and Noller, 2000). Calibrations based on a comparison of ribosome crystal structures with the cleavages generated by numerous Fe(II)-ribosomal-protein derivatives have shown that the distance between the cleavage site and the $\alpha$ carbon of the mutated amino acid is up to 25, 35, or 50 Å for strong, medium, and weak cleavages, respectively (Lancaster et al., 2002). For mapping the PTB binding orientation, we focused on the strong and medium cleavages, because these will arise from high occupancy PTB binding with the RNA reasonably close to the relevant RBD residue, which will not be the case for most, if not all, of the weak cleavages.

## Mapping the Cleavage Sites

Figure 3C summarizes cleavage site data from over 35 such experiments with end-labeled IRES probes (including probes lacking Domains D–G), or more than 60 gels (because the cleavage products of many experiments were analyzed on two gels, differing in the percentage of acrylamide and/or running time), for the 9 Fe(II)-PTB derivatives that consistently gave the strongest signals. Where a given mutant produced cleavages in a number of adjacent phosphodiester bonds (as is usually the case, except for some very weak cleavages), for clarity a single arrowhead (sized according to cleavage efficiency) is used to indicate either the strongest signal or the central cleavage site in cases in which there was little difference in signal strength. The cleavage sites were highly reproducible and were initially assigned using the RNase T1 and alkaline hydrolysis ladders, with verification provided by a few analyses using reverse transcription with six different primers (data not shown), taking advantage of the higher resolution of this approach.

The positions of these nine mutations in the relevant RBDs are depicted in Figure S1, which includes (in the legend) a brief summary of the cleavage patterns generated by the other seven mutants. As is clear from Figure 1C and Figure S1, our assignment of N432 to RBD3 is somewhat arbitrary, because it is actually in the middle of the short linker between RBD3 and RBD4. Because the RNA is thought to be able to loop around between these two RBDs (Oberstrass et al., 2005), N432 is close enough to give some medium cuts (though no strong cleavages), which, in some cases (e.g., in Domain E), are located between sites cut by the other RBD3 mutants (N395 and E419) and the RBD4 mutants, R491 and E518 (Figure 3C).

It is immediately obvious from Figure 3C that the strong-medium cleavages generated by all mutants in a particular RBD are closely clustered in the conventional two-dimensional secondary structure map of the EMCV IRES, implying that PTB binds to the IRES in a limited number of orientations, possibly a unique orientation. Nevertheless, for each RBD, there are clearly at least two, if not three, such clusters: for both RBD1 and RBD2 in Domains F and K; RBD3 in Domains D/E, H, and L; and RBD4 in Domains E/F and G and the base of Domain I. Possible explanations for these multiple clusters are examined in the following two sections.

We repeated these probing assays in the presence of the C-terminal two-thirds fragment of eIF4GI and ATP, with or without eIF4A also present because this enhances the binding of eIF4G to Domain J-K (Kolupaeva et al., 2003). No difference in the pattern of cleavages generated by the Fe(II)-PTB derivatives was seen, only a general slight decrease in signal intensity (data not shown). Probing in the presence of PTB-depleted reticulocyte lysate (i.e., under translation assay conditions) proved impossible because lysates have such high catalase activity.

A striking, and somewhat surprising, feature evident in Figure 3C is the absence of cuts in Domain I (apart from the extreme base of this domain). This was confirmed in assays in which the cleavage products were analyzed by using reverse transcription from nt 754, 606, and 498 (i.e., three primers): although these clearly revealed the customary strong/medium cleavages in Domains G and H, no cleavage product bands were detected in Domain I, apart from t the bottom of this domain

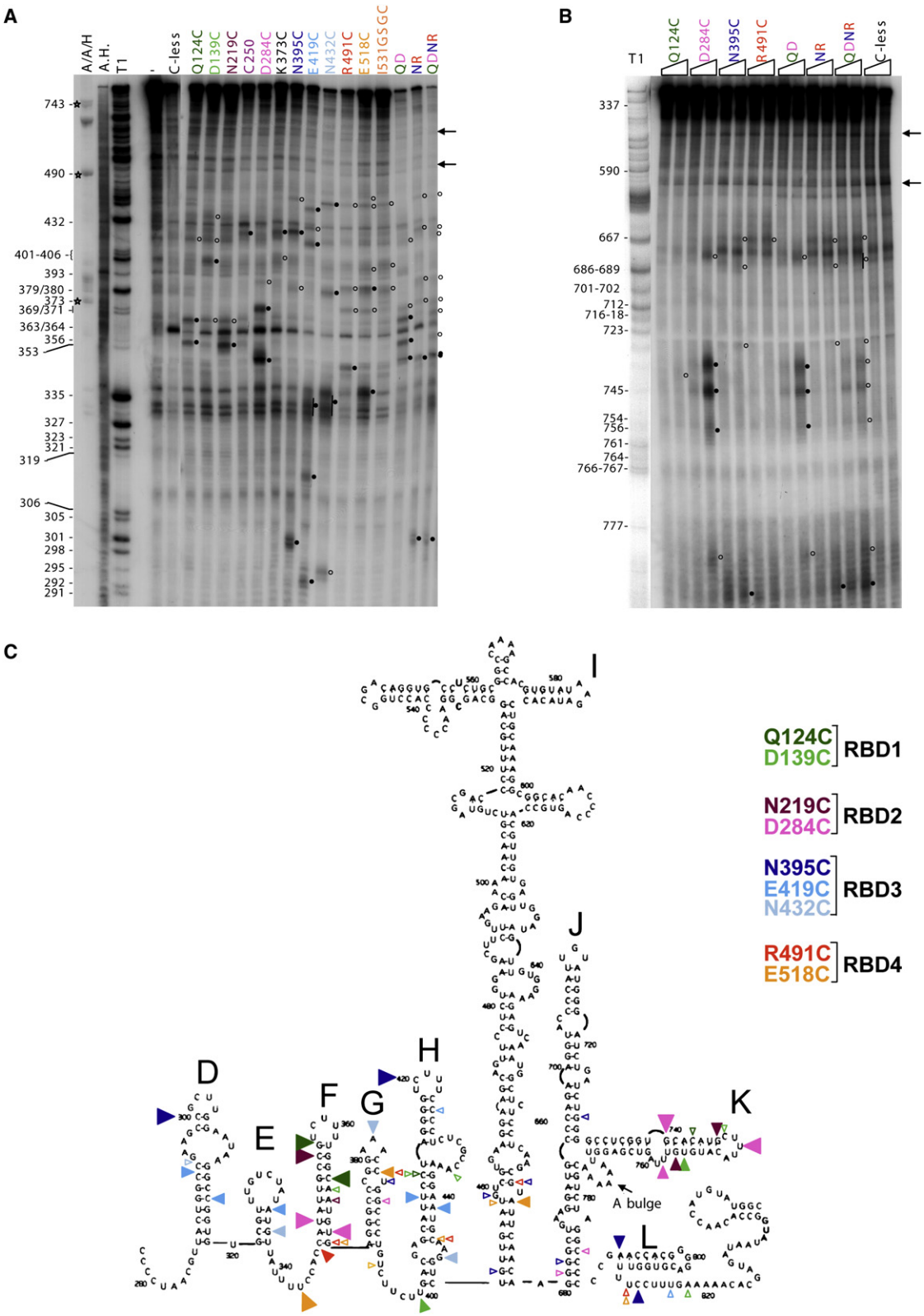


**Figure 3. Hydroxyl Radical Probing of EMCV IRES with Fe(II)-BABE PTB Mutants**

(A) 5′-end $^{32}$P-labeled EMCV-IRES RNA (50 nM) was incubated with 100 nM of the specified derivatized ΔNTD-PTB mutants, or without any protein added (–). The RNA cleavage products were analyzed by urea/polyacrylamide electrophoresis, and the resulting autoradiograph is presented. The RNA fragments

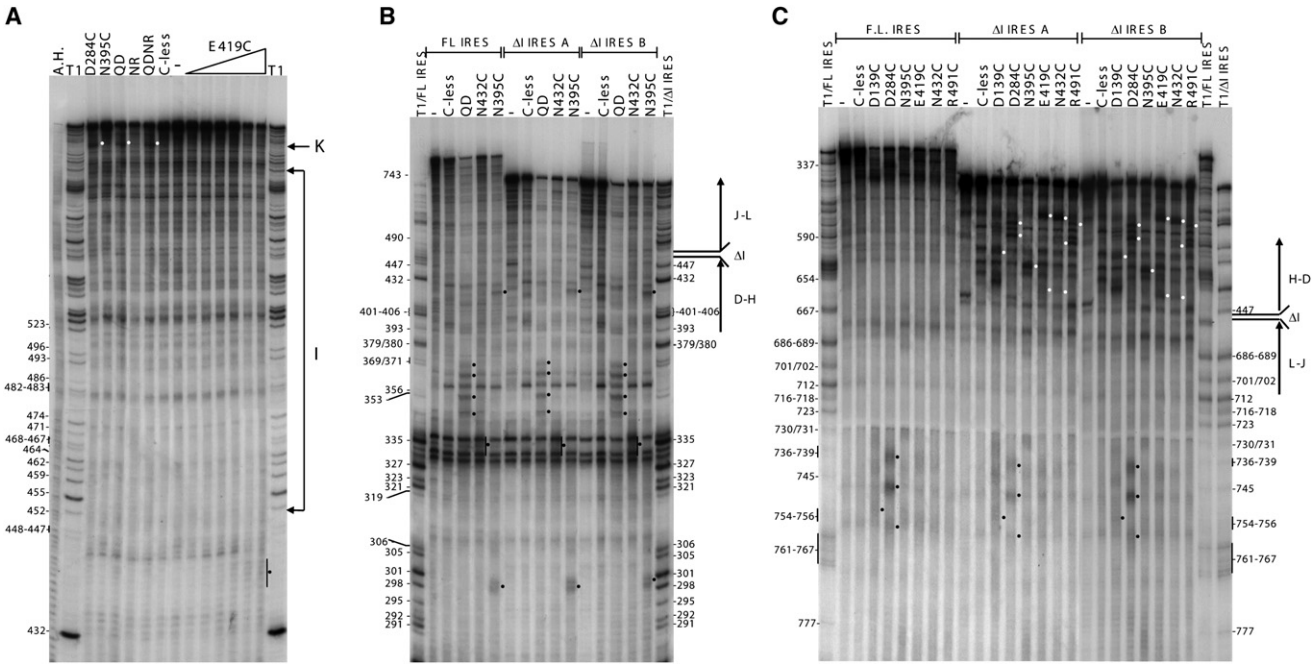


**Figure 4. Domain I Does Not Interact with PTB and Is Not Required for the Interaction of PTB with Other Regions of the IRES**

(A) A 5′-end $^{32}$P-labeled ΔD–G IRES probe (50 nM) was incubated with 100 nM of the designated Fe(II)-ΔNTD-PTB mutants, or with 20, 40, 50, 100, 200, or 300 nM Fe(II)-E419C, or without any PTB (–). RNA fragments generated by directed hydroxyl radical cleavage are indicated as in Figure 3; white symbols are used for clarity where the background is very dark. The region of the gel spanned by Domain I and the cleavages in Domain K are indicated on the right.

(B) 5′-end $^{32}$P-labeled RNA probe (50 nM), either the full-length EMCV IRES, or two different ΔI versions of this RNA (A and B, as defined in Experimental Procedures) were incubated with 100 nM Fe(II)-ΔNTD-PTB mutants or without any protein added (–). The RNA fragments produced by hydroxyl radical cleavage were analyzed by urea/polyacrylamide electrophoresis, and the resulting autoradiograph is presented.

(C) As (B), but with 3′-end-labeled RNAs.

(data not shown). In another approach to reveal cleavages in Domain I, a 5′-end-labeled probe representing just Domains H–L (with Domains D–G deleted) was used, but although the majority of the cleavages in the 3′ side of Domain H were visible at the bottom of the gel, as was the strong cleavage given by D284C in Domain K at the top, no fragments resulting from cutting in Domain I were seen in the middle of the gel (Figure 4A).

We went on to make two deletions removing most of Domain I, but in both cases leaving a short stem-loop in an attempt to maintain the same spatial relationship between the upstream Domains D–H and the downstream Domains J–L as in the full-length IRES. These deletions made no difference to the cleavages in Domains D–H detected with the 5′-end-labeled probe (Figure 4B), nor those in Domains J–L seen with the 3′-end-labeled probe (Figure 4C). Moreover, in the latter case, many of the strong cleavages seen in Domains E–H were also clearly visible (Figure 4C).

We conclude that there are no close contacts between any of the four RBDs of PTB and the major part of Domain I, and that deletion of the majority of Domain I does not appear to significantly perturb the interaction of PTB with the remainder of the IRES, suggesting that Domain I may be relatively independent and spatially separate from the other IRES domains.

## Evidence for Different Affinities of PTB/IRES Interactions at Different Sites

There are three possible explanations for why mutants in any one RBD cause cleavage at two or more widely separated sites

produced by hydroxyl radicals were identified by their absence from the lane with the C-less mutant. Products of strong and medium cleavages are indicated by filled circles on the right-hand side of the track to which they relate, and weak cleavages by open circles. Unmarked bands were considered to be insufficiently stronger than the background signal (Cys-less control lane) to be unambiguously scored as genuine hydroxyl radical cleavage products. Vertical lines are used to indicate consecutive cuts. T1 RNase (T1) and alkaline hydrolysis (A.H.) ladders were also included, and A/A/H is a mixture of run-off transcripts of the EMCV IRES plasmid previously cut with ApaI, ApaLI, or HindIII (the respective RNA transcripts are indicated by stars). The invariant background bands used as "reference standards" for normalization in the determination of cleavage signal strength are highlighted by arrows.

(B) Probing 3′-end $^{32}$P-labeled EMCV IRES RNA (50 nM) was carried out as in (A), except that the Fe(II)-PTB mutants were used at a final concentration of both 50 nM and 100 nM. The resulting autoradiograph is shown, with the fragments resulting from cleavage by hydroxyl radicals highlighted as in (A).

(C) Schematic representation of the location of hydroxyl-radical cleavages in EMCV IRES produced by Fe(II)-PTB derivatives. The predicted secondary structure shown is as presented in Kaminski and Jackson (1998). Cleavage strength assessed as described in the text is indicated as strong (large, filled arrowhead), medium (medium-sized, filled arrowhead), or weak (smallest open arrowhead). Evaluation of cleavage strength by Q124C took into account the fact that conjugation with Fe(II)-BABE was only ~60% complete.

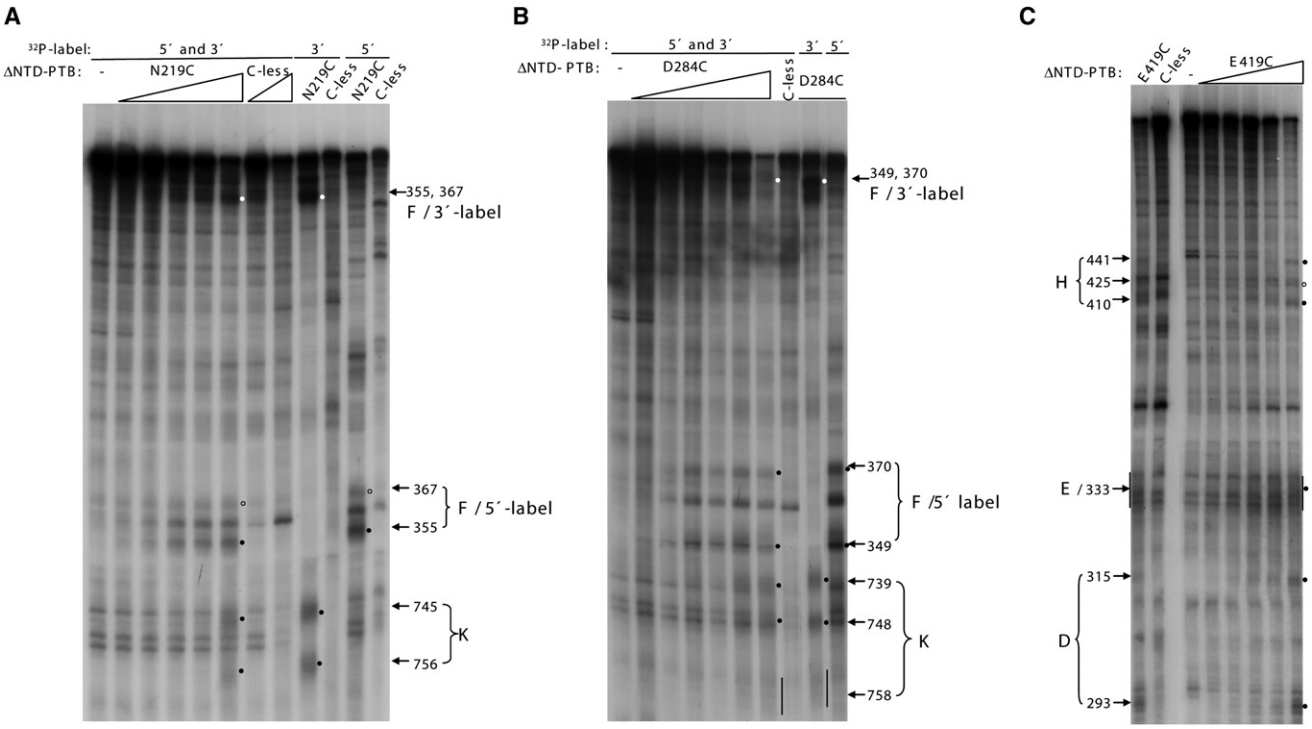


**Figure 5. Directed Hydroxyl Radical Probing Evidence for Different Affinities of the Fe(II)-PTB/IRES Interaction in Different IRES Domains**

(A) EMCV IRES RNA (50 nM) labeled at both ends was incubated with 10, 20, 40, 50, or 100 nM Fe(II)-N219C, or with 10 and 100 nM Cys-less ΔNTD-PTB mutants. In addition 5′-end-labeled and 3′-end-labeled IRES RNAs were incubated (separately) with 100 nM either Fe(II)-N219C or Cys-less mutants. Cleavages in Domains F and K are indicated, as in Figure 3.

(B) Double-labeled IRES RNA (as in [A]) was incubated with 10, 20, 40, 50, 100, and 200 nM Fe(II)-D284C, or with 100 nM Cys-less ΔNTD-PTB mutant. In addition 5′-end-labeled and 3′-end-labeled IRES RNAs were incubated (separately) with 100 nM Fe(II)-D284C. Cleavages in Domains F and K are indicated.

(C) 5′-end-labeled EMCV IRES RNA was incubated at 50 nM with 20, 40, 50, 100, and 200 nM Fe(II)-E419C or with 100 nM Cys-less ΔNTD-PTB mutants. Cleavages in Domains D, E, and H are indicated.

(Figure 3C): (1) the IRES may bind two (or more) PTBs simultaneously; (2) the IRES may bind only one PTB, but in two (or more) alternative orientations; or (3) the IRES may be binding only a single PTB in a unique orientation, but the three-dimensional tertiary structure of the IRES brings into close proximity the (apparently) distant clusters of cleavage sites specific for any one RBD. In an attempt to distinguish between these possibilities, we examined the influence of PTB concentration on the cleavage signals produced by two selected mutants in RBD2 (N219C and D284C), which generate strong or medium cleavages in both Domain F and Domain K (Figure 3C). In order to allow the cleavages in both domains to be examined in a single reaction and in a single gel track, the probe was end labeled at both ends, with markers provided by using probes labeled uniquely at either end. With both derivatives, the cleavage signals in Domain F were already nearly maximal at 40 nM Fe(II)-PTB, whereas the signals in Domain K were only detectable at the higher concentration of 100 nM PTB (Figures 5A and 5B), implying that RBD2 binds with higher affinity to Domain F than to Domain K.

In addition, hydroxyl radical probing of a 5′-end-labeled RNA with increasing amounts of E419C showed that cleavages produced in Domain D were more than half-maximal at 50 nM, whereas those in Domain H started appearing only at 100 nM (Figure 5C), implying a higher-affinity interaction of RBD3 with Domain D than Domain H. All of these observations suggest that the full-length IRES can bind two PTBs simultaneously (but with different affinities), although binding a single PTB in two alternative orientations is not absolutely ruled out.

## Direct Evidence for the Binding of More than One PTB to the Full-Length IRES

Because the EMCV IRES is too large to give band shifts sharp enough to unambiguously determine the stoichiometry of PTB/IRES interactions by EMSAs, we turned to the much more precise method of mass spectrometry. For this, PTB/IRES complexes were initially assembled in 58 mM ammonium acetate (pH 7.4), 2 mM $Mg^{2+}$, with RNA at 10 μM, followed by buffer exchange into 100 mM ammonium acetate (except in the case of the ΔD–I probe, where the PTB/RNA complexes dissociated under the conditions of reduced $Mg^{2+}$ and raised $NH_4^+$) with 2-fold dilution. Wild-type ΔNTD-PTB was used for these experiments at a nominal input molar ratio of 0.5:1, 1:1, or 2:1 with respect to IRES RNA. In view of the fact that the total RNA concentration (after dilution) was 250-fold greater than in the in vitro translation assays (or 100-fold greater than for directed hydroxyl radical probing), and given that estimates of the $K_D$ of the interaction between PTB and various Type II picornavirus IRESs all fall in

the 20–50 nM range (Song et al., 2005), we consider that the nominal 1:1 PTB/RNA input ratio will approximate most closely to the degree of saturation of the RNA with bound PTB pertaining in the translation and probing assays.

The results with four different IRES derivatives (each with 16 nt viral coding sequence at the 3′-end) fall into two classes. The ΔD–G IRES and the more severely truncated ΔD–I version each bound just a single PTB at equimolar input of PTB and RNA (Figures 6B, 6D, and 6F), differing only inasmuch as it was uniquely the complex with the ΔD–I probe that dissociated during the buffer exchange step.

In contrast, the ΔI and full-length IRESs both formed predominantly 2PTB/IRES complexes at nominal equimolar PTB and RNA input (Figures 6A, 6C, and 6F), and this identical behavior confirms that there is no significant PTB binding to Domain I (apart from the base of this domain, which was retained in the ΔI mutants). At a nominal 0.5:1 PTB/RNA input, these IRESs formed only 1:1 complexes, but in considerably higher yield than the ΔD–G and ΔD–I IRESs (Figure 6E). These results strongly imply that under the conditions of the in vitro translation assays and the directed hydroxyl radical probing, the full-length IRES binds 2 PTBs, one to the Domain H–L region, and the other to Domains D–G.

## DISCUSSION

The precise stoichiometries of PTB binding determined by mass spectrometry strongly support the conclusions drawn from the titration experiments of Figure 5, which showed that PTB binds with higher affinity to Domains D and E than to Domains H and K. Putting this information together with the strong and medium cleavage data of Figure 3C allows us to unambiguously map the orientation of PTB binding to the IRES (Figure 7A). One PTB interacts with Domains D–F, with RBD1 and RBD2 interacting with Domain F, and RBD3 and RBD4 with Domains D and E. Another PTB binds with somewhat lower affinity (Figure 5) to the Domains H–L region, with RBD1 and RBD2 contacting Domain K, RBD3 apparently in close proximity simultaneously to Domain H and the base of Domains I and L, and RBD4 appearing to interact only with the base of Domain I (Figure 7A). (It is not clear which PTB causes the cuts in Domain G.)

Our conclusions agree well with previous conventional footprinting data on PTB interactions with Type II picornavirus IRESs (Figure 7B), if the underlying parameters of the different methods are considered, as well as the fact that the probes used in this earlier work all lacked at least Domains D and E (in some cases also Domains F and G). Protection of the RNA against attack by small chemical reagents (e.g., DMS or CMCT) will occur only where there is extremely close contact with the actual RNA-binding surface of the RBD, whereas RNA sites that are protected against ribonucleases (RNase ONE, RNase T1, or RNase VI), but not against DMS or CMCT, are likely to be flanking these sites of intimate contact, much as our approach will generate cleavages at sites flanking the close contact sites, rather than at the direct contact points themselves. Notably, no protections in Domain I were seen in any of these previous footprinting assays.

Given that Domains D–G are not strictly required for IRES function (Jang and Wimmer, 1990; Duke et al., 1992), and that PTB has been shown to stimulate the function of the minimal IRES (Domains H–L), this stimulation must be dependent on the PTB that binds to Domains H–L. How does this interaction stimulate IRES functionality? It seems likely that each base-paired IRES domain is individually rather stable, but the predicted secondary structure (which is rather robust because it is supported by a wealth of phylogenetic data) suggests that the bonds between neighboring domains will have sufficient potential for free rotation to act as hinges, so that the three-dimensional spatial orientation of the base-paired domains, and hence the distances between their apical loops, will be quite flexible or "floppy." The binding of a single PTB to the apical regions of Domain K via RBD1 and RBD2 (Figure 7A), and of Domain H via RBD3 (with probable contact also with the base of Domain L), will clearly place limitations on the interdomain distances and orientations that can be adopted, in effect tethering these domains together, thereby constraining and stabilizing the three-dimensional spatial relationship between Domains H, K, and L. This stabilization of the appropriate structure plausibly explains the stimulatory effect of PTB, as has been suggested previously (Kaminski and Jackson, 1998), but without any direct evidence. The argument was based on the fact that the dependency of EMCV IRES functionality on PTB ranges from virtually no dependence when a wild-type IRES with a 6A residue bulge at the J-K junction (Figure 7) is driving translation of viral coding sequences, to high dependence if the IRES has an enlarged 7A bulge and there is a heterologous reporter (Kaminski and Jackson, 1998), with the size of the bulge having a greater influence than reporter identity. In the case of the 6A bulge, the appropriate spatial relationship between Domains H, K, and L presumably occurs with a high probability, almost by default, with no strong requirement for stabilization by PTB. Although most of our probing was done with the wild-type 6A-IRES, in comparative assays we saw no radical change in the pattern of cleavages with the 7A-IRES, except that the signals generated in Domain K by D139C (RBD1) and D284C (RBD2) were consistently less intense (data not shown). This suggests that the additional residue in the A-rich bulge subtly alters the exact position of Domain K relative to the rest of the IRES, which might have a negative influence on IRES activity unless it is compensated by the binding of PTB.

As for the influence of coding sequences on the PTB dependence of IRES functionality, we examined the effect of appending the first ~160 nt of the viral Leader peptide coding sequences, or an equivalent length of 5′-proximal CAT sequences. These extensions made no difference to the pattern of hydroxyl radical cleavages within the IRES itself. Specific cleavages within the extension indicative of the binding of an additional PTB were seen with viral coding sequences (Figure S2), but not with the CAT coding region. Mass spectrometry confirmed that additional PTB-binding sites were created when these viral coding sequences were appended to the ΔD–I IRES (Table S2). Thus, the higher apparent dependence of IRES activity on added PTB when the IRES is driving CAT expression (Kaminski and Jackson, 1998) cannot be explained by high-affinity binding of PTB to the CAT coding sequences, but might conceivably reflect binding of residual PTB in the PTB-depleted lysate to the viral Leader peptide coding region.

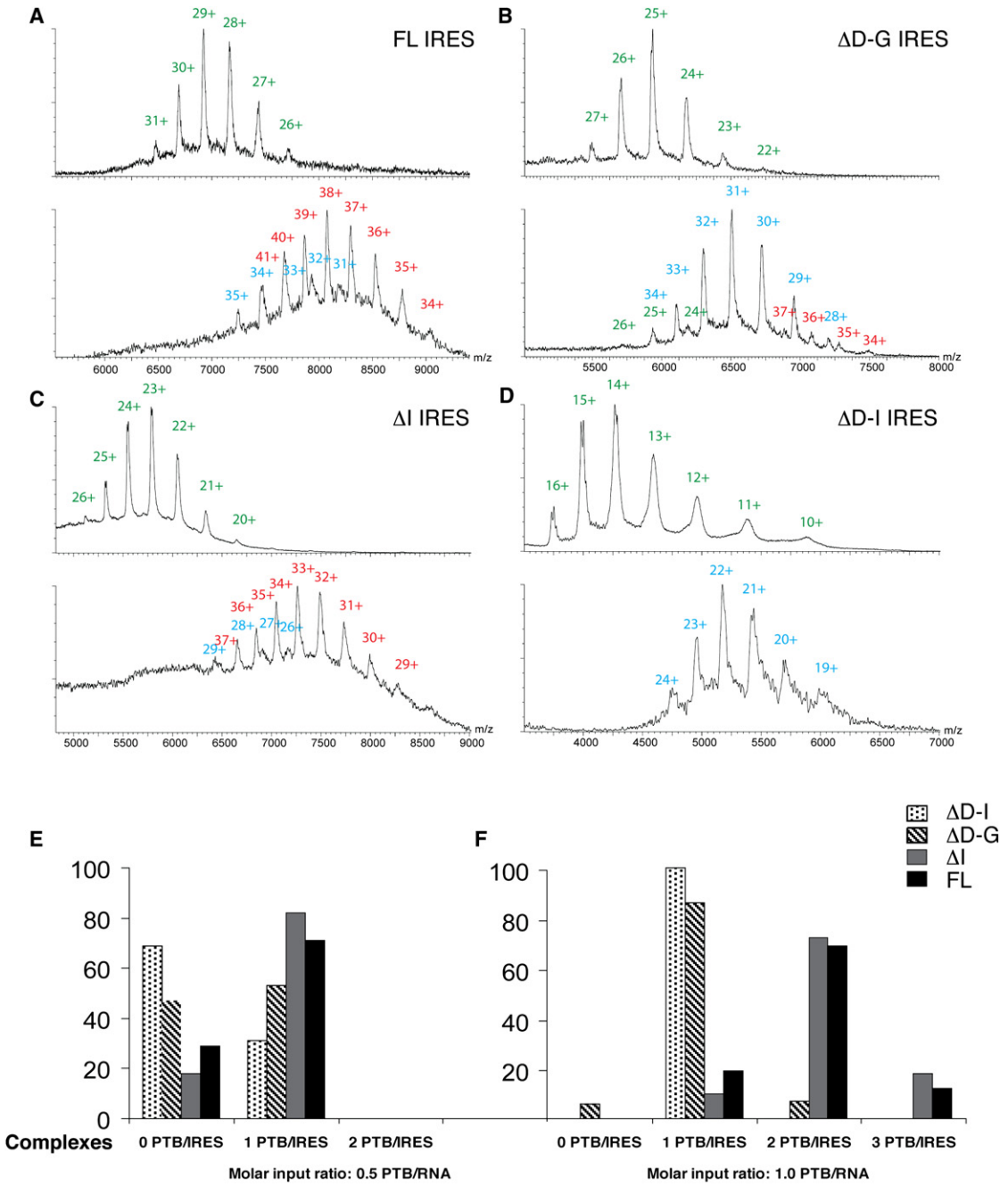


**Figure 6. Mass Spectra of RNA:PTB Complexes Formed on Different IRES Variants**

(A–D) Representative spectra obtained with the RNA alone (upper panels) and with the complexes obtained at a nominal PTB/RNA molar input ratio of 1:1 (lower panels) are shown for: (A) full-length (FL) IRES; (B) ΔD–G IRES; (C) ΔI IRES; and (D) ΔD–I IRES. The charge states are shown in green for the RNA, in blue for the 1:1 complex, and in red for the 2:1 PTB/RNA complex. Because the complexes between PTB and the ΔD–I IRES dissociated during attempts at buffer exchange, this step was omitted and the 1 mM $Mg^{2+}$ present in these samples caused broadening of the peaks. Up to four spectra (minimum of two) were obtained for each IRES at this equimolar PTB/RNA input ratio, and also at ratios of 0.5 and 2.0.

(E and F) The relative proportions of free RNA, 1PTB/RNA, 2PTB/RNA, etc. complexes observed at (E) a nominal molar input ratio of 0.5 PTB/RNA or (F) equimolar PTB and RNA for the four different IRES RNAs: ΔD–I (stippled); ΔD–G (cross-hatched); ΔI (solid gray); and full-length (solid black). Note that the results imply that the actual input PTB/RNA molar ratios were higher than the nominal values, perhaps because the Bradford assay underestimated the true protein concentration, in which case the same (proportional) underestimate will apply to all of the PTB input concentrations with all IRESs.

There has been just one previous attempt to solve the orientation of PTB binding to a Type II IRES (Song et al., 2005), in this case the FMDV IRES. The approach mainly involved UV-crosslinking assays (plus some band shifts) with a range of IRES deletion mutants lacking specific domains, and a series of PTB deletion mutants each lacking one RBD, or two neighboring RBDs. The conclusion agreed with our results with regard to RBD3 binding to Domain H, but differed in most other respects: no contacts between RBD3 and the base of Domain I or L were detected; RBD4 was claimed to bind to Domains J and K; no specific contacts between either RBD1 or RBD2 and the IRES were detected (by UV crosslinking), although RBD2 (but not RBD1) made a strong contribution to the stability of the PTB-IRES interaction (Song et al., 2005). Although the discrepancies might conceivably reflect differences between the EMCV and FMDV IRESs, it seems much more likely that they are due to difficulties associated with the approach that was taken. First, as the authors point out, the absence of UV crosslinking does not necessarily mean an absence of binding, but merely an absence of crosslinkable contacts. Second, the approach assumes that each RBD acts independently, but recent evidence indicates that RBD3 and RBD4 are structurally linked as a coordinated pair (Oberstrass et al., 2005); thus, deletion of either of them would put the other in a structural context quite different from the situation in the full-length protein. Third, deletion of RBD2 would alter the spacing between RBD1 and RBDs 3/4.

Overall, we believe that the directed hydroxyl radical probing approach is far less subject to caveats and potential artifacts. Over the past ~15 years, it has been used quite extensively to map interactions of proteins (RNA polymerases, transcription factors, repressors, etc.) with promoters, to determine the positions and orientations of ribosomal proteins within the ribosome, and to map the interactions of initiation, elongation, and termination factors with ribosomes. By contrast, there have been relatively few investigations into binary protein-RNA interactions. One interesting exception is the binding of the central domain of eIF4GI to the EMCV IRES, which revealed interaction with the upper part of IRES Domain J, and the region around the three-way junction between Domains J and K (Figure 7), but, significantly, not with the distal part of Domain K (Kolupaeva et al., 2003), where PTB RBD1 and RBD2 bind.

As this work has shown, two things make the approach particularly suitable for detailed mapping of how PTB interacts with picornavirus IRESs. First, the NMR structures of each PTB RBD complexed with an oligonucleotide (Oberstrass et al., 2005) allow for a robust, rational choice of sites for Cys substitution: over 80% of these Cys residues were accessible to Fe(II)-BABE, and in all of these cases, the Fe(II) was near enough to the RNA to generate cleavages, yet far enough from the actual RNA-binding surface not to interfere greatly with activity in translation assays. Second, as explained above, the secondary structures of picornavirus IRESs are well established, even though the three-dimensional structures remain enigmatic. Nevertheless, this work has clearly shown that it is essential to know the stoichiometry of the PTB/RNA interactions, and for this purpose mass spectrometry offers the huge advantage of precise quantitation of the relative proportions of each species of complex.

Using mass spectrometry in conjunction with directed hydroxyl radical probing, we have been able to establish that a single PTB binds to the minimal EMCV IRES in a way that would stabilize the three-dimensional fold. This offers the first direct evidence for how PTB binding can stimulate IRES activity, and why the size of the A-rich bulge influences the degree of stimulation. Now that the general approach and our library of mutants have been validated, we anticipate that they will prove extremely useful for investigating PTB interactions with other picornavirus IRESs, with the numerous cellular mRNA IRESs that have been reported to be PTB-dependent (Sawicka et al., 2008), and with pre-mRNAs that are subject to alternative splicing regulated by PTB.

## EXPERIMENTAL PROCEDURES

### Plasmids

The starting constructs for expression of N-terminally His-tagged full-length (FL) PTB1, PTB1-1234 (renamed ΔNTD-PTB for this work), FL-PTB1-C23S, and FL-PTB1-C250S/C251S are as described by Monie et al. (2005). Construction of FL Cys-less PTB1 and Cys-less ΔNTD-PTB, the introduction of a silent HpaI site into the latter (Figure 1B), and the introduction of single Cys residues at the sites shown in Figure 1C were carried out as described in Supplemental Data.

pEMCV L-VP0, with the wild-type 6A bulge or mutant 7A bulge, and pEMCV NS (7A bulge) were as described in Kaminski and Jackson (1998). pΔD–G and pΔD–I were generated by PCR of pEMCV L-VP0. Construction of the ΔI IRESs (with the bulk of Domain I deleted) is described in detail in Supplemental Data. In brief, they both consist of Domains D–H, up to and including nt 455 (Figure 3C) fused via a short linker, either 5′-CGCGCAAGCG-3′ in ΔIA or 5′-AGCTCCGGCT-3′ in ΔIB, to Domains J–L from nt 674 extending to 16 nt past the authentic initiation codon. All of the plasmid constructs were verified by sequencing.

### Purification of PTB Mutants

His-tagged PTB mutants were expressed in *E. coli* M15 cells. Cell pellets were lysed in 300 mM NaCl, 50 mM $NaH_2PO_4$ buffer (pH 8.0), and His-tagged proteins were purified by using Ni-Sepharose 6 Fast-flow from GE Healthcare, Amersham, according to the supplier's instructions. The purified proteins were eluted with 300 mM NaCl, 50 mM $NaH_2PO_4$ (pH 8.0), 350 mM imidazole, in the presence of an EDTA-free protease inhibitor cocktail (Roche), and dialyzed against H100 buffer (20 mM HEPES-KOH [pH 7.5], 100 mM KCl, 2 mM DTT, 5% glycerol). In all cases, the purified protein was at least 95% pure, as verified by Coomassie staining of SDS polyacrylamide gels.

### In Vitro Transcription/Translation Assays

Rabbit reticulocyte lysate (treated with micrococcal nuclease) was depleted of PTB by affinity chromatography. The affinity matrix was prepared by transcription of a plasmid constructed by PCR amplification of EMCV- L-VP0 from the polyC tract to nt 450 in the numbering system of Duke et al. (1992), with primers that would create an XbaI site at the 5′ end and a SacI site at the 3′ end. This fragment was inserted between the XbaI and SacI sites of pSP64Poly(A)-T7 vector (Ali et al., 2001), such that in vitro transcription after linearization with EcoRI would produce IRES Domains D–H with a 3′-poly(A) tail, which was used for affinity depletion as described by Ali et al. (2001) for eIF4G depletion. Monocistronic mRNAs for use in translation assays were generated by T7 RNA polymerase transcription of the plasmid pEMCV NS linearized with EcoRI as described previously (Kaminski and Jackson, 1998). Translation assays were carried out as described previously (Kaminski et al., 1995).

### End Labeling of IRES RNA

All EMCV IRES constructs were linearized with NcoI just downstream of the authentic initiation codon, prior to transcription by T7 RNA polymerase under

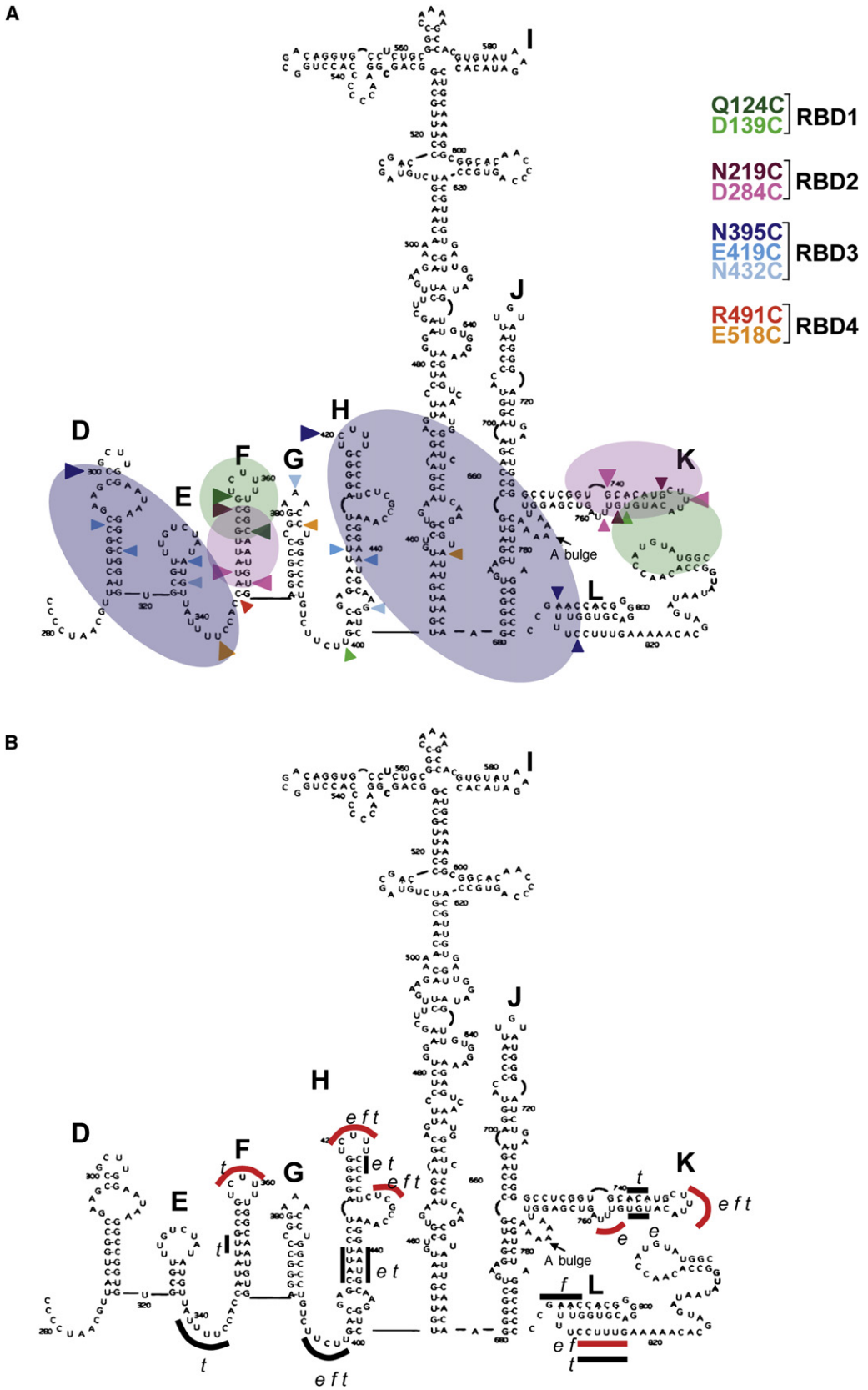
A
B
Q124C
D139C
RBD1
N219C
D284C
RBD2
N395C
E419C
N432C
RBD3
R491C
E518C
RBD4
A bulge
e f t

the following conditions (50 μl final volume): 40 mM Tris-HCl (pH 8.0); 1 mM spermidine; 22 mM $MgCl_2$; 0.05% Triton X-100; 5 mM DTE; 4 mM (each) ATP, CTP, GTP, UTP; 2 mM ApG dinucleotide; and a trace of [$\alpha$-$^{32}$P]UTP (GE Healthcare or Perkin-Elmer) added to the reaction to allow for determination of RNA yield, as described by Kaminski et al. (1995). The transcripts were gel purified in urea/5% polyacrylamide gels and eluted overnight in 500 mM $NH_4OAc$, 10 mM $Mg(OAc)_2$, 0.1 mM EDTA, and 0.1% SDS. After $^{32}$P end labeling (as described in Supplemental Data), 5′-labeled RNA was purified by using Probequant G-50 (GE Healthcare), followed by ethanol precipitation, and 3′-labeled RNA was purified by gel electrophoresis as described above.

### Preparation of Fe(II)-BABE-Derivatized PTB Proteins

Conjugation of Fe(II)-BABE to PTB mutants and purification of the derivatized proteins from unreacted reagent was done essentially as described by Culver and Noller (2000). Briefly, Fe(II)-BABE (120 nmol) was incubated with 2 nmol PTB mutant protein in 80 mM HEPES-KOH, 100 mM KCl, 5% glycerol (pH 7.5) in a final volume of 150 μl at 37°C for 30 min. Excess Fe(II)-BABE was removed by ultrafiltration with Microcon YM-30 concentrators (Amicon) at 4°C and 5000 rpm, followed by three washes with 400 μl buffer. Mock derivatization of the Cys-less ΔNTD-PTB was also performed as a control for possible derivatization of nonCys residues. The efficiency of derivatization was estimated by running the proteins (~400 ng) on a 10% SDS-PAGE.

### Directed Hydroxyl Radical Probing

2.5 pmol of $^{32}$P-end-labeled IRES RNA was heated briefly at 95°C, snap cooled after the addition of binding buffer (80 mM HEPES-KOH, 100 mM KCl, and 2 mM $MgCl_2$ [pH 7.4]), and incubated (in a total volume of 50 μl) for 15 min at 37°C with the appropriate amount of Fe(II)-PTB mutant (usually 5 pmol). The reaction was then put on ice, and 1 μl 250 mM freshly prepared ascorbic acid and 1 μl 1.25% $H_2O_2$ were added, to initiate the Fenton reaction. After a 30 min incubation on ice, the RNA was reisolated by phenol extraction and ethanol precipitation, and the fragments were analyzed by urea-acrylamide (5%–8%) gel electrophoresis, followed by autoradiography.

### Nanospray Mass Spectrometry of PTB/IRES Complexes

The IRES RNA was heated to 95°C for 3 min and immediately diluted to 10 μM in assembly buffer (58 mM ammonium acetate and 2 mM magnesium acetate [pH 7.4]), followed by addition of the appropriate amount of PTB. After incubation at 37°C for 15 min and cooling on ice, the material was buffer exchanged into 100 mM ammonium acetate (except for the ΔD–I RNA) by using micro Bio-Spin Chromatography Columns (Bio-Rad, UK) with a 6 kDa cut-off, and diluted in this buffer to give 5 μM total RNA, preparatory to mass spectrometry. In the case of samples with the ΔD–I probe, mass spectrometry was carried out after 2-fold dilution with 100 mM ammonium acetate. NanoESI spectra were acquired on a Q star (MDS Analytical Technologies) modified for optimized performance at high masses (Sobott et al., 2002; Chernushevich and Thomson, 2004). For a comparison of the experimentally determined masses of the RNA probes and the theoretical values, see Table S1.

## SUPPLEMENTAL DATA

Supplemental Data include three tables, two figures, Supplemental Experimental Procedures and can be found with this article online at http://www.cell.com/molecular-cell/supplemental/S1097-2765(09)00268-8.

## ACKNOWLEDGMENTS

We thank Ann Kaminski, Clare Gooding, and Harry Noller for helpful advice, and Jenny Reed for technical support. This work was supported by Biotechnology and Biological Sciences Research Council Project Grants BB/E0048571 to R.J.J. and BB/F0103111 to C.V.R.

Received: December 5, 2008
Revised: February 26, 2009
Accepted: April 13, 2009
Published: June 11, 2009

## REFERENCES

Ali, I.K., McKendrick, L., Morley, S.J., and Jackson, R.J. (2001). Truncated initiation factor eIF4G lacking an eIF4E binding site can support capped mRNA translation. EMBO J. *20*, 4233–4242.

Chernushevich, I.V., and Thomson, B.A. (2004). Collisional cooling of large ions in electrospray mass spectrometry. Anal. Chem. *76*, 1754–1760.

Culver, G.M., and Noller, H.F. (2000). Directed hydroxyl radical probing of RNA from iron(II) tethered to proteins in ribonucleoprotein complexes. Methods Enzymol. *318*, 461–475.

Duke, G.M., Hoffman, M.A., and Palmenberg, A.C. (1992). Sequence and structural elements that contribute to efficient encephalomyocarditis virus RNA translation. J. Virol. *66*, 1602–1609.

Ghetti, A., Pinolroma, S., Michael, W.M., Morandi, C., and Dreyfuss, G. (1992). hnRNP-I, the polypyrimidine tract-binding protein: distinct nuclear localization and association with hnRNAs. Nucleic Acids Res. *20*, 3671–3678.

Hunt, S.L., and Jackson, R.J. (1999). Polypyrimidine-tract binding protein (PTB) is necessary, but not sufficient, for efficient internal initiation of translation of human rhinovirus-2 RNA. RNA *5*, 344–359.

Jackson, R.J., and Kaminski, A. (1995). Internal initiation of translation in eukaryotes: the picornavirus paradigm and beyond. RNA *1*, 985–1000.

Jang, S.K., and Wimmer, E. (1990). Cap-independent translation of encephalomyocarditis virus RNA: structural elements of the internal ribosome entry site and involvement of a cellular 57-kD RNA-binding protein. Genes Dev. *4*, 1560–1572.

Kaminski, A., and Jackson, R.J. (1998). The polypyrimidine tract binding protein (PTB) requirement for internal initiation of translation of cardiovirus RNAs is conditional rather than absolute. RNA *4*, 626–638.

Kaminski, A., Hunt, S.L., Patton, J.G., and Jackson, R.J. (1995). Direct evidence that polypyrimidine tract binding protein (PTB) is essential for internal initiation of translation of encephalomyocarditis virus RNA. RNA *1*, 924–938.

Kolupaeva, V.G., Hellen, C.U.T., and Shatsky, I.N. (1996). Structural analysis of the interaction of the pyrimidine tract-binding protein with the internal ribosomal entry site of encephalomyocarditis virus and foot-and-mouth disease virus RNAs. RNA *2*, 1199–1212.

Kolupaeva, V.G., Lomakin, I.B., Pestova, T.V., and Hellen, C.U.T. (2003). Eukaryotic initiation factors 4G and 4A mediate conformational changes downstream of the initiation codon of the encephalomyocarditis virus internal ribosomal entry site. Mol. Cell. Biol. *23*, 687–698.

Lancaster, L., Kiel, M.C., Kaji, A., and Noller, H.F. (2002). Orientation of ribosome recycling factor in the ribosome from directed hydroxyl radical probing. Cell *111*, 129–140.

**Figure 7. Docking PTB onto the EMCV IRES**

(A) Strong and medium cleavages caused by the nine designated Fe(II)-PTB derivatives are shown as in Figure 3C. The deduced orientation of PTB binding is shown in the same color code: transparent green denotes RBD1, RBD2 is pink, and the RBD3+4 di-domain is transparent blue.

(B) Comparative results of previous conventional footprinting (protection) assays of PTB binding to Type II picornavirus IRESs. Sites protected by PTB binding against reaction with DMS and CMCT are shown in red; sites that are not protected against DMS or CMCT, but are protected against cleavage by RNase ONE, or RNase T1 or RNase VI, are shown in black. Sites protected in the three IRESs are indicated as follows: (e) EMCV (Kolupaeva et al., 1996); (f) FMDV (Kolupaeva et al., 1996; Pilipenko et al., 2000); and (t) Theiler's murine encephalomyelitis virus (Pilipenko et al., 2001). Only the TMEV IRES probe included Domain F; the EMCV IRES probe had Domain G at its 5′ end and the FMDV IRES Domain H.

Marzi, S., Knight, W., Brandi, L., Caserta, E., Soboleva, N., Hill, W.E., Gualerzi, C.O., and Lodmell, J.S. (2003). Ribosomal localization of translation initiation factor IF2. RNA *9*, 958–969.

Monie, T.P., Hernandez, H., Robinson, C.V., Simpson, P., Matthews, S., and Curry, S. (2005). The polypyrimidine tract binding protein is a monomer. RNA *11*, 1803–1808.

Niepmann, M. (1996). Porcine polypyrimidine tract-binding protein stimulates translation initiation at the internal ribosome entry site of foot-and-mouth-disease virus. FEBS Lett. *388*, 39–42.

Oberstrass, F.C., Auweter, S.D., Erat, M., Hargous, Y., Henning, A., Wenter, P., Reymond, L., Amir-Ahmady, B., Pitsch, S., Black, D.L., and Allain, F.H.T. (2005). Structure of PTB bound to RNA: specific binding and implications for splicing regulation. Science *309*, 2054–2057.

Pilipenko, E.V., Pestova, T.V., Kolupaeva, V.G., Khitrina, E.V., Poperechnaya, A.N., Agol, V.I., and Hellen, C.U.T. (2000). A cell cycle-dependent protein serves as a template-specific translation initiation factor. Genes Dev. *14*, 2028–2045.

Pilipenko, E.V., Viktorova, E.G., Guest, S.T., Agol, V.I., and Roos, R.P. (2001). Cell-specific proteins regulate viral RNA translation and virus-induced disease. EMBO J. *23*, 6899–6908.

Sawicka, K., Bushell, M., Spriggs, K.A., and Willis, A.E. (2008). Polypyrimidine-tract-binding protein: a multifunctional RNA-binding protein. Biochem. Soc. Trans. *36*, 641–647.

Sobott, F., Hernandez, H., McCammon, M.G., Tito, M.A., and Robinson, C.V. (2002). A tandem mass spectrometer for improved transmission and analysis of large macromolecular assemblies. Anal. Chem. *74*, 1402–1407.

Song, Y., Tzima, E., Ochs, K., Bassili, G., Trusheim, H., Linder, M., Preissner, K.T., and Niepmann, M. (2005). Evidence for an RNA chaperone function of polypyrimidine tract-binding protein in picornavirus translation. RNA *11*, 1809–1824.

Valcarcel, J., and Gebauer, F. (1997). Post-transcriptional regulation: the dawn of PTB. Curr. Biol. *7*, R705–R708.

Wollerton, M.C., Gooding, C., Robinson, F., Brown, E.C., Jackson, R.J., and Smith, C.W.J. (2001). Differential alternative splicing activity of isoforms of polypyrimidine tract binding protein (PTB). RNA *7*, 819–832.